Geomechanics and Engineering, *Vol. 26, No. 4 (2021) 369-384*
https://doi.org/10.12989/gae.2021.26.4.369

Arching effect in sand piles under base deflection using geometrically non-linear isogeometric analysis

Tan Nguyen[1] and Loc V. Tran*[2]

[1]Sustainable Developments in Civil Engineering Research Group, Faculty of Civil Engineering, Ton Duc Thang University, Ho Chi Minh City, Vietnam
[2]Faculty of Civil Engineering, Ton Duc Thang University, Ho Chi Minh City, Vietnam

(Received December 30, 2020, Revised July 17, 2021, Accepted August 5, 2021)

Abstract. Arching effect is a universal phenomenon of the load transfer mechanism which is visually observed in the heaps of granular material. In this study, we adopt geometrically non-linear isogeometric finite element analysis to revisit the theoretical concept of the arching effect in the granular sand piles under base deflection with an assumption of elastic continuum theory. Through two studies of the planar and conical sand heaps, this work expects to supply the numerical results for double-checking some simple benchmarks before extending to the complicated problems. Herein, the reliability and accuracy of the present model are validated by checking the weight balance condition and comparing with some available literature. The numerical results demonstrate that the stress dip accompanying a significant shear stress mobilization at the base is formed immediately once the base deflection occurs. Furthermore, the trajectories of principal stresses are plotted to visually manifest the force propagation in the sand piles which enables us to explain the formation and shape of the arching effect.

Keywords: arching effect; base deflection; geometric non-linearity; sand piles; stress dip

1. Introduction

The arching effect firstly proposed by Terzaghi (1943) is a universal phenomenon of the load transfer mechanism. In this phenomenon, the peak pressure at the base of bulk solids might not locate at the center which has the greatest material height. It is confirmed through several experiments (Smid and Novosad 1981, Pipatpongsa *et al.* 2014) that the pressure distribution is in form of an M-shape, wherein the magnitude lost at the center approximately 40% as compared to the hydrostatic pressure for a 2m – high stockpile (McBride 2006), which can be called with a “pressure dip” term. Study of pressure dip significantly impacts in engineering practice, ranging from the bulk solid stockpiles of mineral industries (McBride 2006, Ai *et al.* 2010) to geotechnical engineering involving foundations, road and tunnel constructions as well as embankments on soft soils (Okamura *et al.* 2013, Meena *et al.* 2020), and so on. Many studies have been carried out to disclose the characteristic of the arching effect by using plenty of methodologies such as experimental (Trollope 1956, Lee 2019), analytical (Lee *et al.* 2016, Jaouhar *et al.* 2018) and numerical approaches (Moradi and Abbasnejad 2015, (Wensrich and Katterfeld 2012, Ai *et al.* 2013, Zhou *et al.* 2014, Horabik *et al.* 2017). An overview can be discussed in the comprehensive review articles (Savage 1998, Atman *et al.* 2005). It is worthwhile noting in Ai *et al.* (2013) that almost all numerical solutions have been based on discrete element modelling (DEM) due to direct simulation of each particle in the bulk solid while finite element methods (FEM) are seldom in use.

Actually, experimental measurements at the laboratory or the project sites are common and easiest. However, this method strongly depends on experiment setup and instrumentations as well. In some cases, the measurement devices, i.e., strain gauges and pressure cells, could affect the desired results. Furthermore, another obvious limitation comes from having to implement a lot of experiment tests to provide complete and sufficient experimental data, resulting in time consumption and highly economical costs (Eltaher *et al.* 2021). Therefore, theoretical solutions are adopted to double-check the stress field in the sand pile by many researchers within additional postulates. For examples, Terzaghi (1943) assumed the sand pile is divided into two separated regions behaving solely either elastic or fully plastic. Wittmer *et al.* (1996) proposed an assumption of fixed principal axes (FPA), whereby the direction of the major compressive stress is fixed under an angle bounded by gravity direction and the angle of repose. Later, through a new model, so-called Oriented Stress Linearity (OSL), Wittmer *et al.* (1997) considered the arching effect in the sand piles as an inclined inter-particle force propagation. Meanwhile, Matuttis and Schinner (1999) adopted a linear superposition of granular cones to evaluate the pressure distribution under granular wedges. Angelillo *et al.* (2016) supplied the analytical solutions for the prismatic sand pile under itself gravity in which the granular material is modeled as a continuum governed by the Mohr-Coulomb yield condition. Moreover, some recent works have been done with a viscoelastic assumption (Abdelrahman *et al.* 2021, Alnujaie *et al.* 2021, Esen *et al.* 2021), in which the

---

*Corresponding author, Ph.D.
E-mail: tranvinhloc@tdtu.edu.vn

http://www.techno-press.org/?journal=gae&subpage=7

ISSN: 2005-307X (Print), 2092-6219 (Online)

soil foundation is modeled as the viscoelastic dampers. On the other hand, Booker (1969) and Nguyen *et al.* (2019) figured out the local minimum pressure in planar and conical sand piles under the a priori condition of passive stress state, in which the material is assumed to be on the verge of incipient failure everywhere. By another way, DEM can directly simulate each particle of bulk solids in different shapes, including spherical and also non-spherical (Matuttis 1998, Zhou *et al.* 2014, Horabik *et al.* 2017). Although DEM can produce consistent results with the experimental tests, it requires an extremely computational cost since the number of particles is huge, for instance, in an assembly of 50.000 spherical particles (Horabik *et al.* 2017) or up to 10^5 particles (Savage 1998). This disadvantage requests alternative approaches that could reduce computing resources while maintaining the numerical performance. Among the promising methods, finite element method (FEM) is a predominant option. Some FEM studies have successfully described the pressure dip underneath the apex at the base of granular materials relying on some complicated elastoplastic models, for instance, the Drucker–Prager model (Modaressi *et al.* 1999), Mohr-Coulomb model (Jeong and Moore 2010). Furthermore, Ai *et al.* (2013) adopted the isotropic constitutive laws with two elastic and three elastic-plastic models. Whilst, Bi (2017) also concluded that the Rayleigh-Ritz method associated with generalized Hooke's law can capture the stress field in the granular soil heaps. Using a similar assumption, Nguyen *et al.* (2018) investigated the stress distribution in the planar sand pile by using isogeometric analysis. All three above numerical solutions are confirmed that the linear elastic continuum theory is feasible to study the problems of granular mechanics. Furthermore, an advantage numerical method, namely numerical manifold method (NMM) (Yang *et al.* 2016) has recently developed and been considered as an effective computational tool for geotechnical engineering related to landslide problems (Yang *et al.* 2019 and Yang *et al.* 2021) and fracture problems (Yang *et al.* 2018 and Wu *et al.* 2020) as well.

In this present paper, we extended Nguyen *et al.* (2018)'s work by adopting the assumption of elastic continuum theory incorporating to large deformation isogeometric finite element approach. Hence, effect of base deflection on the sand piles behavior is investigated with some aspects and limitations:

- Firstly, we simplify a real three-dimensional sand pile to the two-dimensional geometry including planar and conical sand heaps, then derive the governing formulations based on an assumption of elastic continuum theory for the granular sand heap. The formulation takes into account the von Kármán strain tensor for geometrical nonlinearity. In many instances, assumptions of linearity lead to reasonable idealization. However, in certain circumstances, e.g., beam (Almitani *et al.* 2020, Esen *et al.* 2020, Bashiri *et al.* 2021), plate (Tran *et al.* 2015) and shell (Li *et al.* 2018) structures, these assumptions deviate from the real response of structures. But it is still a big question whether how large deformation does affect the geotechnical problems, e.g., the sand heaps.
- Secondly, finite element modelling based on isogeometric analysis (IGA) proposed by Hughes *et al.* (2005) is adopted for discretizing the above problems. Herein, the present method has an advantage in exactly describing the profile of base deflection in form of a parabolic equation. Besides some salient features of IGA exhibits some bottleneck in local refinement (Nguyen *et al.* 2015). Interestingly, this drawback is naturally overcome by using T-spline functions (Nguyen-Thanh *et al.* 2011) or combining with meshfree collocation method (Nguyen-Thanh *et al.* 2019; Nguyen-Thanh *et al.* 2020). This enhanced method is promising to provide an effective computational tool for some complex geometry or stress concentrated problems e.g. embankments, dams (Savage 1998). In this study, the geometry nevertheless is still simple as a triangular due to the real shape of the cross-section of the sand piles. Therefore, this work is expected to supply the numerical results for double-checking some simple benchmarks before extending to complicated cases.
- Thirdly, the effect of the base deflection on the stress dip and the arch formation in the sand piles is investigated. As proposed in Wittmer *et al.* (1997), the shape of the arch can be revealed as the rotation of the force chain which could be alike to the trajectory of the most compressive principal stress in a continuous medium (Peters *et al.* 2005). The conjugate relationship between the stress dip and the force chain in planar sand piles has been successfully demonstrated by Oron and Herrmann (1998) using an exact calculation of the force networks. On the other hand, Handy (1985) successfully drawn the shape of soil arching action by showing the path of minor principal stress of soil behind the retaining wall. In the sand piles, although the stress dip has been found, the shape of the arching effect has not been comprehensively determined.
- Finally, we analyze the characteristic of the local stress dip caused by the base deflection in the sand piles then unify the concept of the arching effect between geotechnical perspective proposed by Terzaghi (1943) and granular physics proposed by Wittmer *et al.* (1997). Indeed, Terzaghi (1943) stated that the arching effect is a transfer of pressure from a yielding mass of soil onto adjoining stationary parts; whereas, Wittmer *et al.* (1997) considered the arching effect in the sand piles resting on a rigid base as inclined inter-particle force propagation. To that end, the formation of arch action is visually manifest following Peter *et al.* (2005)'s suggestion by revealing the stress dip and the trajectory of the most compressive principal stress as well.

2. Physical problem

2.1 Geometry and boundary condition

In this study, axisymmetric conical and symmetric planar sand piles are simultaneously considered. The sand piles have the height of h=1m and are stabilized under the repose angle ϕ=30°. A rectangular coordinate is imposed on the sand piles in which the origin is located at the center of the bottom of the sand piles, the abscissa axis (x) horizontally points toward the right-hand side of the piles while the ordinate axis (y) points upward in the

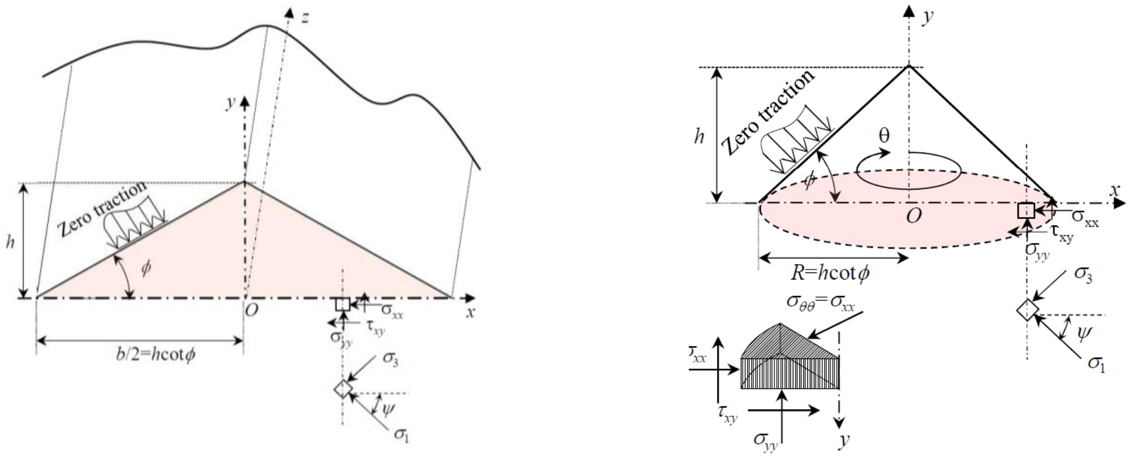

(a) A symmetric planar sand pile (b) An axisymmetric conical sand pile

Fig. 1 Geometry and stress components of sand piles

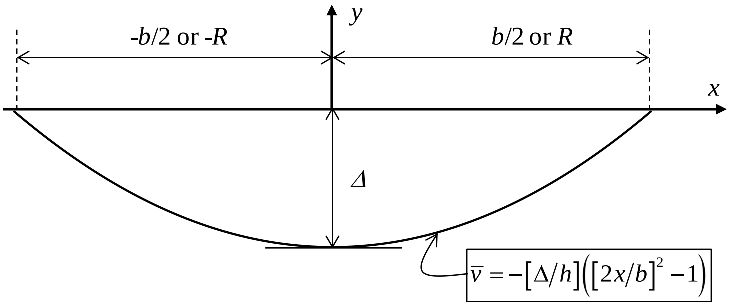

Fig. 2 Parabolic shape of the base deflection

gravitational direction. In addition to the three rectangular stress components (σ_{xx}, σ_{yy}, and τ_{xy}) using for the planar sand pile, the conical sand pile can be modelled in two dimensions by considering an additional circumferential stress component ($\sigma_{\theta\theta}$). The sign convention of stress is adopted from soil mechanics in which the compressive stress is positive. The geometry and stress components of planar and conical sand piles are shown in Fig. 1(a) and Fig. 1(b), respectively.

Herein, angle between the direction of the major principal stress and the positive horizontal axis, denoted as ψ which is calculated as follows

$$\tan(2\psi) = \frac{2\tau_{xy}}{\sigma_{xx} - \sigma_{yy}} \tag{1}$$

The base deflection is imposed under concave parabolic curvature as shown in Fig. 2.

2.2 Theoretical formulation

Let consider, in general, a three-dimensional solid defined in a domain the static equilibrium equation can be written in partial differential form as

$$\sigma_{ij,j} + b_i = 0 \ \ in \ \Omega \quad \text{with} \quad i, j = 1, 2, 3 \tag{2}$$

Note that the subscript commas is the partial differential meanwhile b_i is the body force and σ_{ij} is the internal stress which is revealed in term of strain ε_{ij} following the constitutive equation as

$$\sigma_{ij} = C_{ijkl}\varepsilon_{kl} \tag{3}$$

where C_{ijkl} is the elasticity tensor of material and can be simplified to be suitable to two-dimensional elastic problems as shown in Fig. 1 ((A2) and (A3) in Appendix).

The in-plane strains are associated with in-plane displacement fields $\mathbf{u} = [u, v]^T$ according to the Green strain assumption as

$$\boldsymbol{\varepsilon} = \boldsymbol{\varepsilon}_L + \boldsymbol{\varepsilon}_{NL}^{\alpha}, \quad \text{where} \quad \alpha := u, v \tag{4}$$

where the linear and nonlinear strain components are defined respectively as

$$\boldsymbol{\varepsilon}_L = \begin{Bmatrix} u_{,x} \\ v_{,y} \\ u_{,y} + v_{,x} \end{Bmatrix} \tag{5}$$

$$\boldsymbol{\varepsilon}_{NL}^{\alpha} = \frac{1}{2}\mathbf{A}_{\alpha}\boldsymbol{\alpha} \quad \text{in which} \quad \mathbf{A}_{\alpha} = \begin{bmatrix} \alpha_{,x} & 0 \\ 0 & \alpha_{,y} \\ \alpha_{,y} & \alpha_{,x} \end{bmatrix} \quad \text{and} \quad \boldsymbol{\alpha} = \begin{Bmatrix} \alpha_{,x} \\ \alpha_{,y} \end{Bmatrix} \tag{6}$$

In which the Greek symbol α denotes the displacement variables as mentioned in Eq. (4).

By being similar to those of plane strain, an axisymmetric solid mathematically behaves also in two dimensions, in which *u* and *v* are displacements along the radial and axial coordinates as displayed in Fig. 1b, respectively. However, unlike the plane strain problem, in the axisymmetric situation, the strain in the circumferential direction is certainly non-zero, i.e. $\varepsilon_{\theta\theta} \neq 0$. Thus, the strain vector in Eq. (4) is expanded from three to four terms as $\hat{\boldsymbol{\varepsilon}} = \{\boldsymbol{\varepsilon}^T \quad \varepsilon_{\theta\theta}\}^T$ which is defined as

$$\hat{\boldsymbol{\varepsilon}} = \begin{Bmatrix} \boldsymbol{\varepsilon}_L \\ u/x \end{Bmatrix} + \begin{Bmatrix} \boldsymbol{\varepsilon}_{NL}^{\alpha} \\ 0 \end{Bmatrix} + \begin{Bmatrix} \mathbf{0} \\ \varepsilon_{NL}^{\theta} \end{Bmatrix} \quad \text{where} \quad \varepsilon_{NL}^{\theta} = \frac{u^2}{2x^2} \qquad (7)$$

As seen in Eq. (7), once $x \longrightarrow \infty$, the circumferential stress becomes zero ($\varepsilon_{\theta\theta} = 0$). Consequently, the plane strain situation can be retrieved. Therefore, the formulation of the axisymmetric problem is merely presented without loss generality.

Then, the virtual work equation for a continuum is expressed according to total Lagrange coordinate as

$$\int_V \delta\hat{\boldsymbol{\varepsilon}}^T \hat{\boldsymbol{\sigma}} \mathrm{dV} = \int_V \delta\mathbf{u}^T \mathbf{b} \mathrm{dV} + \int_\Omega \delta\mathbf{u}^T \mathbf{f}_s \mathrm{d}\Omega \qquad (8)$$

where *V* is the undeformed volume and while **b** and $\mathbf{f}_s$ are the body forces and the surface tractions applied over the area *Ω*, respectively.

3. Method of geometrically non-linear isogeometric analysis

In this section, the method of isogeometric analysis and its manipulations for the geometrically nonlinear planar and conical sand piles are briefly introduced.

3.1 Basic function

Be a specific case of the finite element method – using the Lagrange basic function - the isogeometric analysis (IGA) utilizes the spline functions (e.g., B-Spline, NURBS, T-Spline, …) as the shape functions. They are defined recursively by using the Cox–de Boor algorithm (Piegl and Tiller 1995) as follows

$$N_i^p(\xi) = \frac{\xi - \xi_i}{\xi_{i+p} - \xi_i} N_i^{p-1}(\xi) + \frac{\xi_{i+p+1} - \xi}{\xi_{i+p+1} - \xi_{i+1}} N_{i+1}^{p-1}(\xi) \qquad p \geq 1$$

$$\text{at} \quad p = 0, \quad N_i^0(\xi) = \begin{cases} 1 & if \quad \xi_i < \xi < \xi_{i+1} \\ 0 & \text{otherwise} \end{cases} \qquad (9)$$

were, knot value $\xi_i \in \mathrm{R}^+$ $i = 1, 2, ..., m + p$ belongs to an open knot vector $\Xi_\xi = \{\xi_1, \xi_2, ..., \xi_{m+p+1}\}$, which is a non-decreasing sequence of parameter values. Meanwhile, *p* and *m* are the polynomial order and number of the basis functions, respectively. Through a pair of knot vectors Ξ_ξ and Ξ_η , bivariate B-splines basis functions are generated according to tensor product scheme given as below

$$N_{i,j}^{p,q}(\xi, \eta) = N_i^p(\xi) M_j^q(\eta) \qquad (10)$$

3.2 Isogeometric finite element formulation

In similarity to the finite element method, the isogeometric analysis also invokes the isoparametric concept. However, unlike the finite element method, IGA utilizes the same basis function from the geometric description to approximate the unknown displacement fields.

$$\mathbf{u}^h(\boldsymbol{\xi}) = \sum_A N_A(\boldsymbol{\xi}) \mathbf{d}_A \qquad (11)$$

where $\mathbf{d}_A = [u_A \; v_A]^T$ denotes a vector of nodal degrees of freedom associated with the control point $\mathbf{P}_A$. By substituting Eq. (11) into Eq. (7), the strain can be rewritten in term of the strain matrices ((A4) and (A5) in Appendix) as

$$\hat{\boldsymbol{\varepsilon}} = \sum_{A=1}^{m \times n} \left(\mathbf{B}_A^L + \frac{1}{2} \mathbf{B}_{\alpha_A}^{NL} + \frac{1}{2} \mathbf{B}_{\theta_A}^{NL} \right) \mathbf{d}_A \qquad (12)$$

By substituting Eq. (12) into Eq. (8), the system of linear static equation is obtained as follows

$$\mathbf{Kd} = \mathbf{F} \qquad (13)$$

where the global stiffness matrix **K** is given by

$$\mathbf{K} = 2\pi \int_\Omega \left(\mathbf{B}^L + \mathbf{B}_\alpha^{NL} + \mathbf{B}_\theta^{NL} \right)^T \mathbf{C} \left(\mathbf{B}^L + 0.5\mathbf{B}_\alpha^{NL} + 0.5\mathbf{B}_\theta^{NL} \right) x \mathrm{d}\Omega \qquad (14)$$

and **F** is load vector

$$\mathbf{F}_A = 2\pi \int_\Omega \mathbf{I} N_A \mathbf{b} x \mathrm{d}\Omega + \int_\Omega \mathbf{I} N_A \mathbf{f}_s \mathrm{d}\Omega \qquad (15)$$

In which, **I** is the identity matrix. As seen in Eqs. (14) and (15), the volume integral is changed to surface integral in calculating the global stiffness matrix and the force vector by multiplying with a term $2\pi x$ because of the axisymmetric situation. The multiplied term is replaced by 1 in the case of the plane strain.

3.3 Inhomogeneous boundary condition enforcement

Unlike the homogeneous boundary conditions (BCs), the displacement gets a non-zero value in the inhomogeneous Dirichlet boundary conditions, for example, the base deflection at the bottom of the sand piles displayed in Fig. 2. By imitating Eq. (11), the prescribed deflection can be exactly described through the basic function and the control variables, v_A at the bottom control net as:

$$v(x_C) = \sum N_A(x_C) v_A \qquad (16)$$

Due to the lack of the Kronecker delta property of the basis function, value v_A does not usually represent a

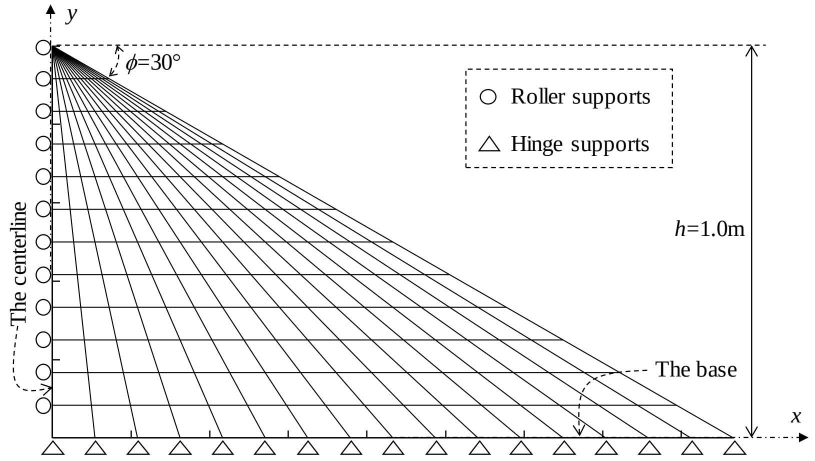

Fig. 3 Physical mesh and boundary conditions of the sand piles

physical nodal displacement as in traditional FEM, especially for the control points located outside the actual domain. As a result, we cannot impose directly the values getting from the base deflection profile for them. Therefore, it is necessary to employ a special technique to estimate the control variables. Some techniques, e.g., the Lagrange multiplier method, the penalty method, the augmented Lagrange method, Nitsche's method are available in an overview in the context of the meshless method (Nguyen *et al.* 2008). In this work, a least square minimization technique in what follows De Luycker *et al.* (2011) is adopted to impose the general inhomogeneous Dirichlet boundary conditions in IGA approximation. The basic idea of this treatment is to minimize the following quantity:

$$J = \frac{1}{2}\sum\left[v(x_C) - \bar{v}(x_C)\right]^2 \tag{17}$$

where $\bar{v}(x_C)$ is the displacement value at a collocation point x_C staying on the essential boundaries.

3.4 Solution procedure

From Eq. (13), it can be seen that the stiffness matrix, **K**, has a nonlinear relation with the unknown displacement vector **d** because $\mathbf{B}^{NL}$ is a function of the displacement field. Thus, to solve the system of the nonlinear equation Eq. (13) we adopted the Newton-Raphson method. Herein, we would like to briefly present the solution procedure. For more details, one can refer to Tran *et al.* (2016), Tran and Niiranen (2020).

Firstly, the governing equation can be rewritten in form of a residual force, which should be zero at the equilibrium state

$$\boldsymbol{\varphi}(\mathbf{d}) = \mathbf{K}(\mathbf{d})\mathbf{d} - \mathbf{F} = 0 \tag{18}$$

However, at the initial state, the displacement vector commonly gives an unbalance residual force, means $\boldsymbol{\varphi}(\mathbf{d}) \neq 0$. Thus, Eq. (18) is solved iteratively, in which the displacement is updated by an incremental displacement $\Delta\mathbf{d}$ until the displacement error between two consecutive iterations reduces below a desired error tolerance, e.g., 0.1%. The incremental displacement $\Delta\mathbf{d}$ is given through the following system of a linear algebraic equation related to the tangent stiffness (A6) as

$$\mathbf{K}_T\Delta\mathbf{d} = -\boldsymbol{\varphi} \tag{19}$$

4. Results and discussion

4.1 Input parameters of the elastic model

The physical mesh of planar and conical sand piles with the height of 1m and the angle of repose ϕ=30° is shown in Fig. 3. The boundary condition at the bottom of the sand piles is fully rough. As consequence, the restrain at the bottom is assigned as a hinge. Regarding the material properties, the value of Young's modulus of loose sand used in a small scale of physical models are chosen in a range of 10^3-10^4 kPa (Girijavallabhan and Reese 1968), for an example, Young's modulus E=2000 kPa and Poisson's ratio μ=0.3 (Ai *et al.* 2013).

4.2 Verification and validation

Firstly, we consider the planar sand pile relying on the assumption of linear continuum elasticity with a rigid base condition for a convergence study. By using two numerical methods of traditional FEM and IGA with their meshes fully plotted in Fig. 4. The maximum vertical stress is occurred at the base and tabulated in Table 1. As seen, both methods well converge to the experimental value of 0.838 from work of Lee and Herington (1971). Interestingly, IGA is faster convergence than FEM with a requirement of 216 cubic elements to achieve 3% error as compared to asking 9600 quadrilateral elements by traditional FEM. Consequently, with a nearly same level of accuracy, IGA requires fewer computing resources. However, for the sake of fairly comparison as considering the same number of elements in use, IGA surely takes much time consumption than FEM due to generating more degree of freedoms and looping more the Gauss points during numerical integration by Gaussian quadrature (Hughes *et al.*

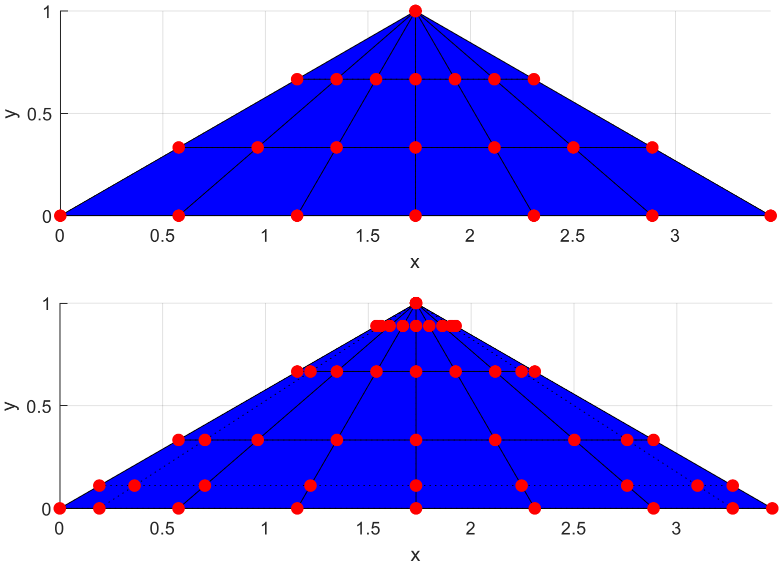

Fig. 4 Fully meshes of 6×3 elements by using the numerical methods: (upper) traditional FEM and (lower) IGA

Table 1 Convergence study and comparison of the efficiency between FEM and IGA

No. of Elements		24	216	600	1176	2400	5400	9600
	$\sigma_{yy}/\gamma h$	0.6772	0.7748	0.7928	0.8000	0.8052	0.8091	**0.8110**
FEM	DoF	72	500	1312	2508	5022	11132	19642
	time (s)	0.68	0.91	1.49	1.84	3.41	9.58	28.43
	$\sigma_{yy}/\gamma h$	0.7974	**0.8103**	0.8128	0.8139	0.8147	0.8153	0.8156
IGA	DoF	132	648	1548	2832	5478	11808	20538
	time (s)	1.51	4.21	4.33	8.16	19.06	60.87	153.90

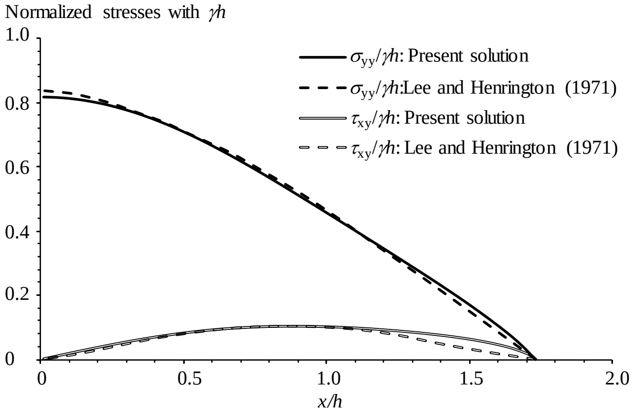

Fig. 5 Comparison of normalized vertical stress with experimental results of (Lee and Herington 1971) for a perfectly rough rigid base with ϕ=30°

Table 2 Discrepancy between the total weight and resultant force on the base of sand piles

Geometries	Δ/h (%)	0	1	2
	Weight (kN)	21.58	21.58	21.58
Planar sand pile	Resultant force (kN)	21.50	21.54	21.62
	Error (%)	0.37	0.21	0.20
	Weight (kN)	39.14	39.14	39.14
Conical sand pile	Resultant force (kN)	38.81	38.95	39.29
	Error (%)	0.86	0.51	0.36

2005). As noted, to gain the computational cost in Table 1, both programs are compiled in a desktop PC with Intel(R) Core (TM) i7-7600U CPU @2.80 GHz and RAM of 16.0 GB.

Next, to validate the present model based on the geometrically non-linear continuum elasticity, the obtained results are compared to other available solutions of the planar and conical sand piles. For the planar problem, Fig. 5 shows an excellent agreement of the vertical stress distributed at the bottom of the sand pile between the present model and the experimental works done by Lee and Herington (1971), Trollope and Burman (1980). Herein, due to symmetric geometry, the result is just plotted at the right half. Meanwhile, a comparison of the stress profiles with the numerical results by Ai *et al.* (2013) for the conical sand pile is revealed in Fig. 6. As seen, although utilizing the linear elastic continuum model, the present model predicts nearly identical vertical stress and slightly smaller shear stress as compared to that of Ai *et al.* (2013) using linear elastic with Mohr-Coulomb plasticity (LEMC) and linear elastic with Drucker–Prager plasticity (LEDP).

Furthermore, the weight balance condition is also checked to validate the numerical model. In essence, the vertical reaction force at the base must be balanced by the total weight of the sand pile. To facilitate the verification, the dry unit weight of sand is selected as γ=12.46 kN/m^3. The result of the comparison is shown in Table 2. As seen, the discrepancies between the resultant forces and the weight of sand pile are less than 0.9% for all cases.

4.3 Stress distribution in planar and conical sand piles resting on a rigid base

As shown in Fig. 7, the vertical and horizontal stresses

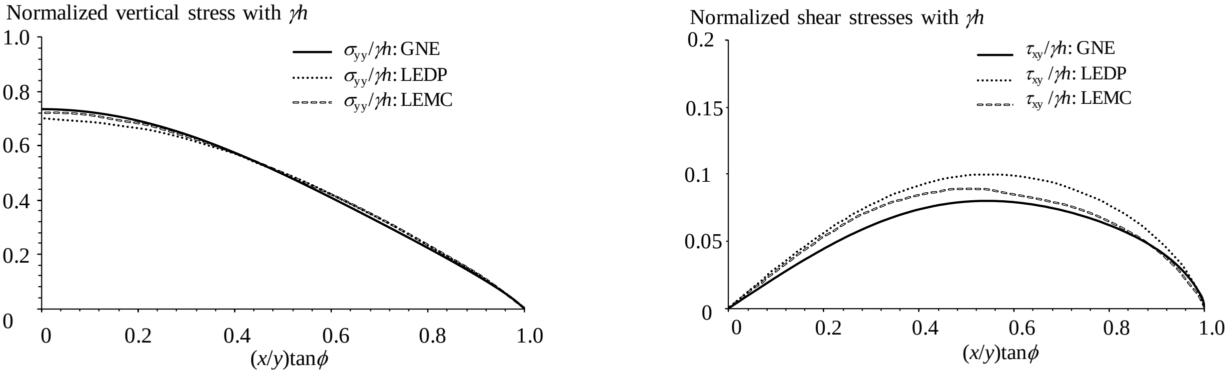

(a) Vertical stress

(b) Shear stress

Fig. 6 Comparison of stress distribution in the sand piles resting on a rigid base with other numerical models (Ai *et al.* 2013)

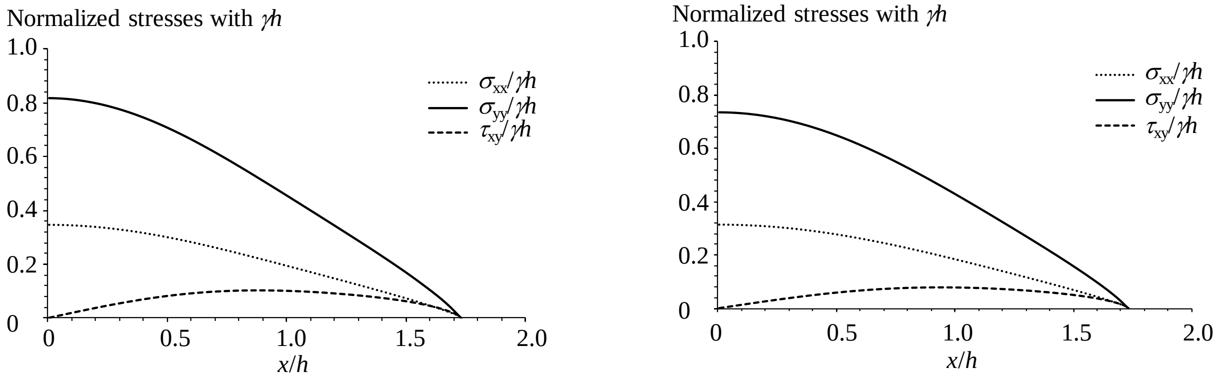

(a) Symmetric planar sand pile

(b) Axisymmetric conical sand pile

Fig. 7 Rectangular stress components in sand pile with rigid base

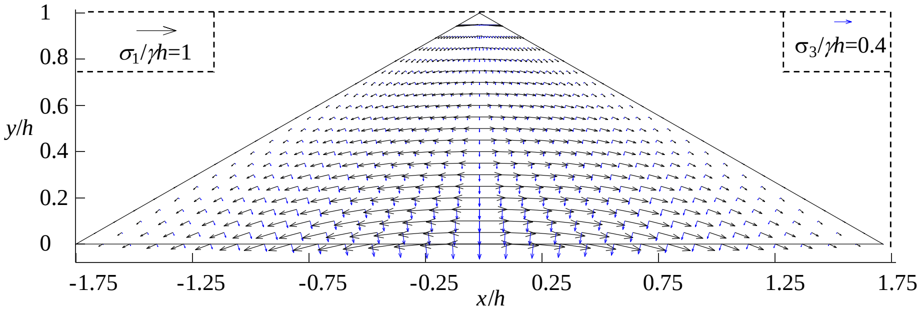

Fig. 8 Trajectories of the principal stresses $\sigma_1/\gamma h$ and $\sigma_3/\gamma h$ in the planar sand pile with Δ/h=0

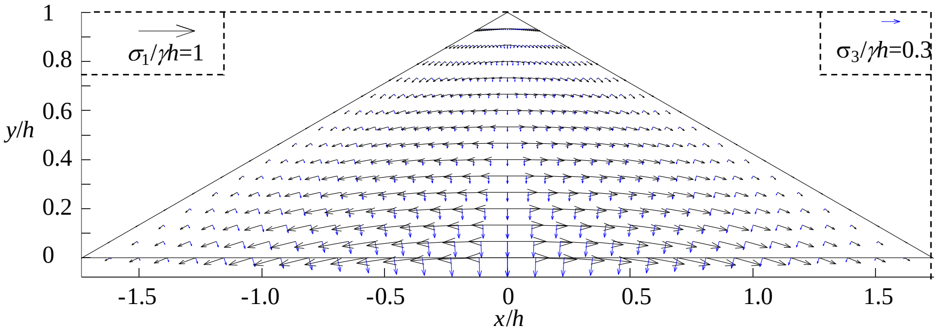

Fig. 9 Trajectories of the principal stresses $\sigma_1/\gamma h$ and $\sigma_3/\gamma h$ in the conical sand pile with Δ/h=0

at the bottom of the sand piles exhibit a humped profile, in which their largest values occur at the centerline underneath the apex of the sand piles. It should be noted that the horizontal stress is proportional to the vertical stress

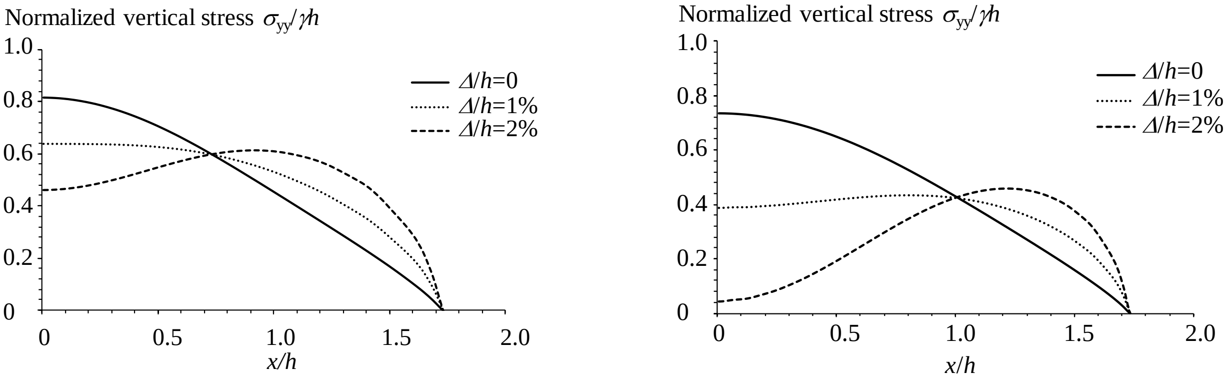

(a) Symmetric planar sand pile (b) Axisymmetric conical sand pile

Fig. 10 Vertical stress redistribution concerning the magnitude of base deflection in the sand piles

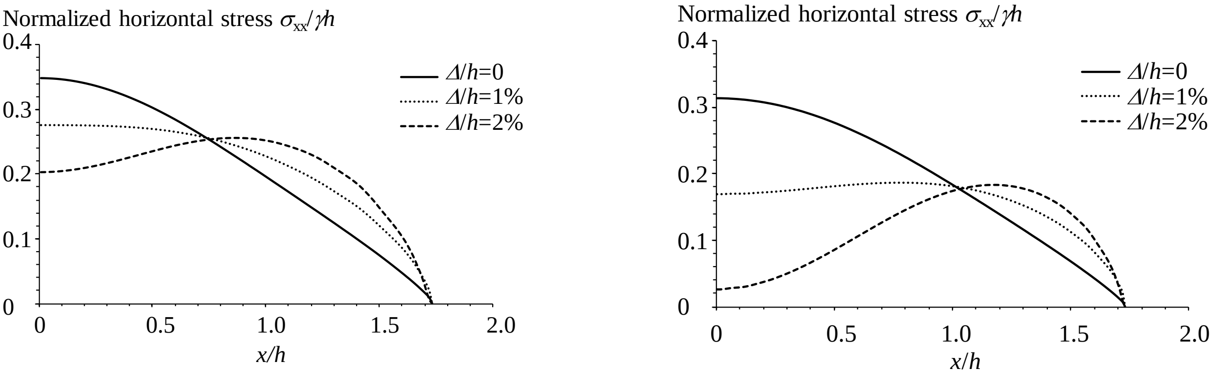

(a) Symmetric planar sand pile (b) Axisymmetric conical sand pile

Fig. 11 Horizontal stress redistribution concerning the magnitude of base deflection in the sand piles

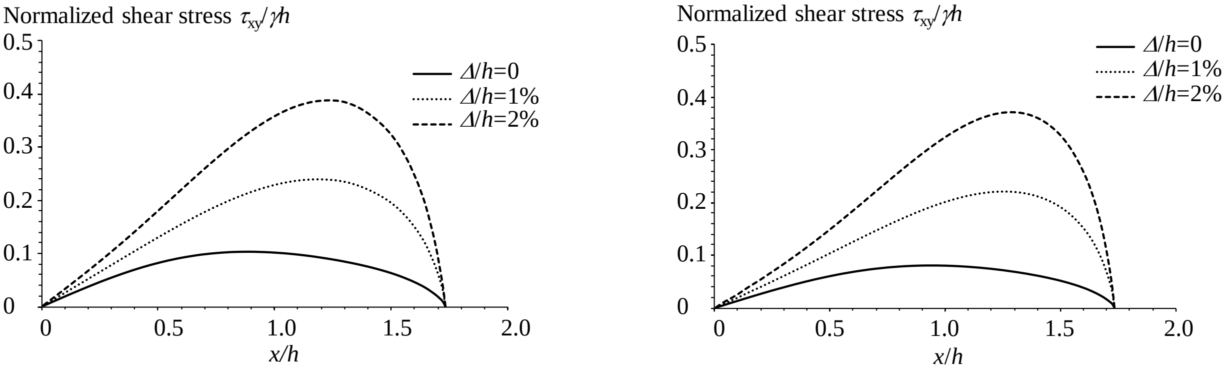

(a) Symmetric planar sand pile (b) Axisymmetric conical sand pile

Fig. 12 Shear stress redistribution with respect to the magnitude of base deflection in the sand piles

through a coefficient in term of Poisson's ratio as $K_o=\mu/(1-\mu)$. Meanwhile, the shear stress is zero at the center and the conners and gains the largest value at a certain point around the bottom edge middle. The shear stress represents the friction force at the bottom which plays a role in stabilizing the sand pile under its gravity.

Furthermore, the trajectories of the principal stresses of the planar and conical sand piles are plotted in Fig. 8 and Fig. 9, respectively. In which, the black arrow denotes the major principal stress which is the largest compression while the blue one stands for the minor one. Obviously, the connected path of the major principal stress demonstrates an arch-line structure. This means its direction is horizontal at the centerline and then gradually tilts diagonally toward the base. These trajectories of the principal stress are alike to those appeared in Parry's work (Parry 1954) but different from studies of Booker 1969 and Nguyen *et al.* 2019 relying the fully plastic analysis where the trajectory path is plotted as a vertical line at the centerline, although the rectangular stresses are the same. Because in the plastic

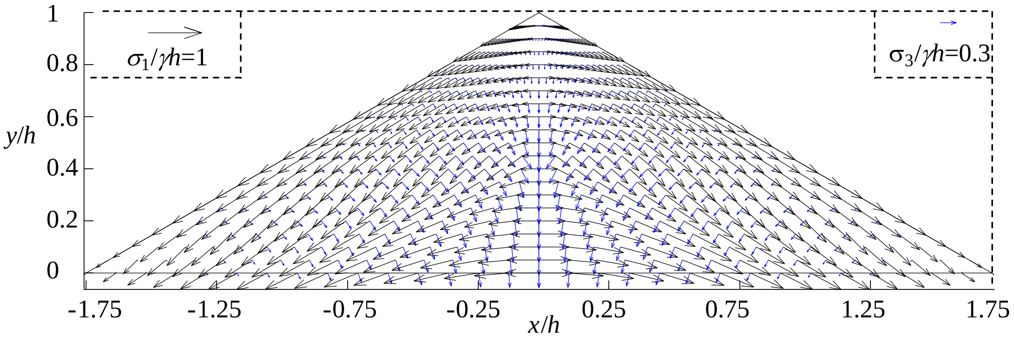

Fig. 13 Trajectories of the principal stresses $\sigma_1/\gamma h$ and $\sigma_3/\gamma h$ in the symmetric planar sand pile with Δ/h=1%

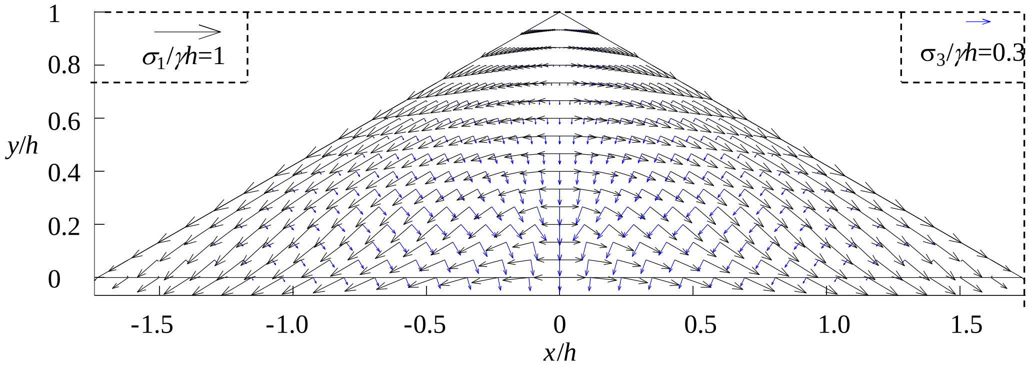

Fig. 14 Trajectories of the principal stresses $\sigma_1/\gamma h$ and $\sigma_3/\gamma h$ in the axisymmetric conical sand pile with Δ/h=1%

model, the sand piles with rigid base stay in an active stress state (Marais 1969, Nguyen *et al.* 2019).

This outcome of the elastic model on the characteristic of force chain, however, is reasonable. Indeed, the humped profile of the vertical stress is achieved at the bottom of the sand piles but the maximum magnitude is considerably smaller than the hydrostatic one γh around 20% and 30% for planar and conical problems, respectively. In essence, the stress relaxation caused by the downward sloping surface of the sand piles might be partially ascribed to the stress reduction. Apart from this, the occurrence of arch formation played the main role in the stress reduction. The shape of the trajectory of the most compressive principal stress shown in Fig. 8 and Fig. 9 is explained as the mass of the sand piles above the central vicinity has slightly transferred to the adjoining parts under an arch-like shape. The arch occurrence is sustained by the shear stress mobilization at the base of sand pile whereby the shear stress is largest at the abutment of the arch. This force chain elaborately elucidates the concept of arching effect in the sand pile prosed by (Wittmer *et al.* 1997). There is no yielding part in these sand piles, but the whole sand piles stated in the stationary condition. Hence, the definition of the arching effect stated by Terzaghi (1943) is difficult to explain the load transfer mechanism in static sand piles.

4.4 Characterization of the rotation of force propagation in the planar and conical sand piles due to base deflection

As imposing the base deflection as shown in Fig. 2 with a value of Δ/h=1% and 2%, the axial stresses at the bottom edge are redistributed as observed in Fig. 10 and Fig. 11. Indeed, the stress drops immediately from a humped profile once Δ/h=0 to a concave curvature profile with a local minimum at the middle when the base deflects. Furthermore, the stress dip is proportional to the magnitude of the basal subsidence. This feature signifies that the mass of sand in the central vicinity has been transferred to the adjoining regions, causing redistribution of the vertical and horizontal stresses with a local minimum at the centerline. Nonetheless, the characteristic of stress drops between such two problems: planar and conical sand piles is distinct. Under the same basal subsidence, the stress drop value in the conical problem is more pronounced (approximately twice) than that of the planar sand pile. It explains why the arching effect takes place more intensively in the conical sand pile as observation in the sand piles resting on the rigid base in which the stress dip is induced by the shape of particles (Liu *et al.* 2017).

In an opposite manner of the normal stresses, the shear stress is redistributed as shown in Fig. 12 with increase in magnitude according to increase in the basal subsidence. In other words, a pronounced stress dip accompanied by substantial shear stress mobilization in the sand piles is found once the base deflects. The conjugate relationship between vertical stress dip and shear stress mobilization is a salient feature of arching formation (Michalowski and Park 2004). It can be concluded that the arching effect has been promoted in the sand piles by imposing the base deflection; nonetheless, they are unable to characterize the formation of the arching effect. Therefore, the path of the major principal

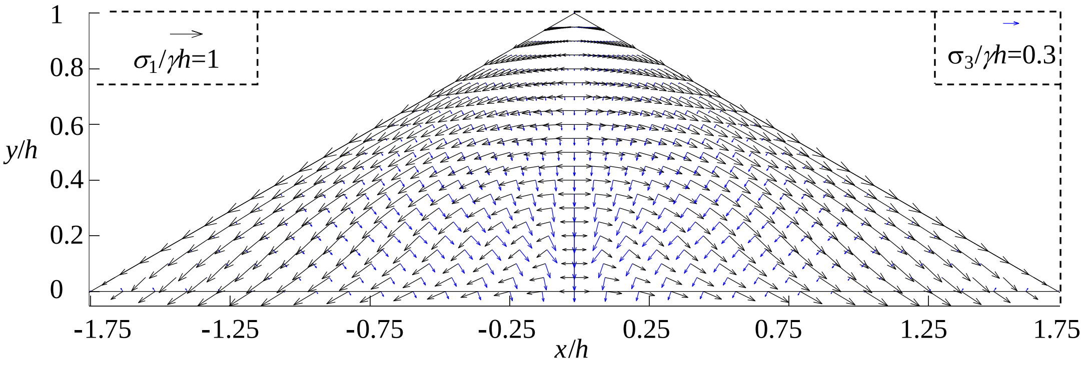

Fig. 15 Trajectories of principal stresses $\sigma_1/\gamma h$ and $\sigma_3/\gamma h$ in the symmetric planar sand pile with Δ/h=2%

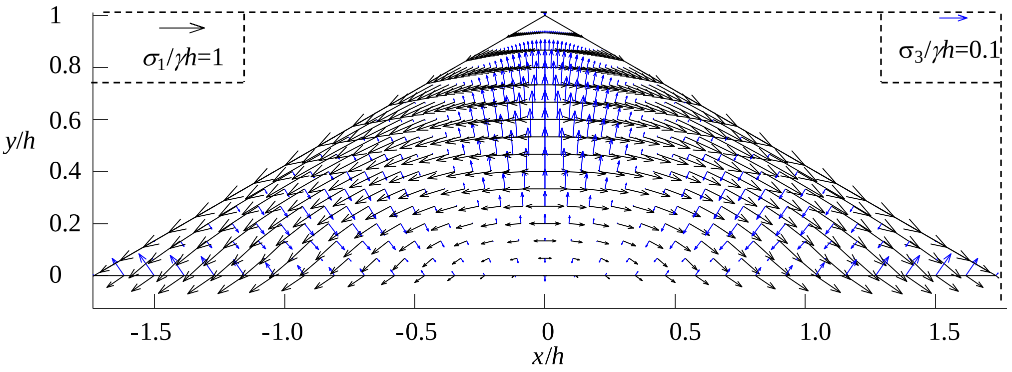

Fig. 16 Trajectories of principal stresses $\sigma_1/\gamma h$ and $\sigma_3/\gamma h$ in the axisymmetric conical sand pile with Δ/h=2%

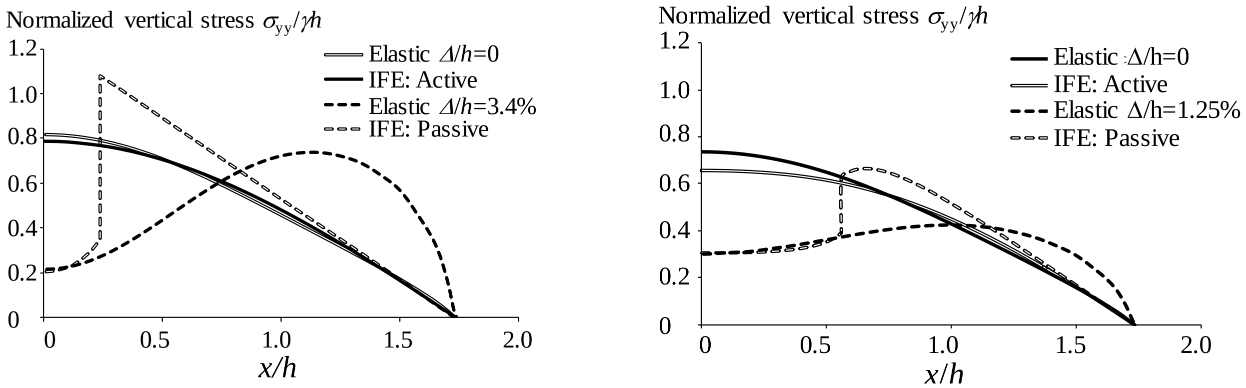

(a) Symmetric planar sand pile

(b) Axisymmetric conical sand pile

Fig. 17 Comparison of stress redistribution in sand piles between non-linear elastic solution and incipient failure everywhere solution

stress has to be taken into account.

Apart from the path of the major principal stresses in the sand piles resting on the rigid base shown in Figs. 8 and 9, the path of the major principal stresses in the sand piles with the basal subsidence of Δ/h=1% and Δ/h=2% are substantially changed as shown in Figs. 13-14 and Figs. 15-16 for planar and conical sand piles, respectively. It looks like the path is rotated more from that of the rigid base. This rotational trait of principal stress could be explained mathematically by determining the angle between the direction of the major principal stress and the positive horizontal axis in Eq. (1). In essence, its magnitude is directly proportional to the shear stress and inversely proportional with the subtraction between axial stresses. As seen in Fig. 10 and 11, the ratio of horizontal and vertical stresses is independent on the base deflection while the shear stress is very sensitive to basal subsidence as shown in Fig. 12. Therefore, the magnitude of the angle of the major principal stress increases according to increase in the magnitude of the base deflection. As a result, the path of the major principal stress becomes steeper and steeper. This explanation could elucidate the definition of the arching effect proposed by Wittmer *et al.* 1997. According to Wittmer *et al.* (1997)'s paper, the mass transfer from one region to other regions results in the inclined force propagation which could be interpreted as the arching effect. The inclination of the force propagation is induced by the shear stress mobilization as above discussion. Hence,

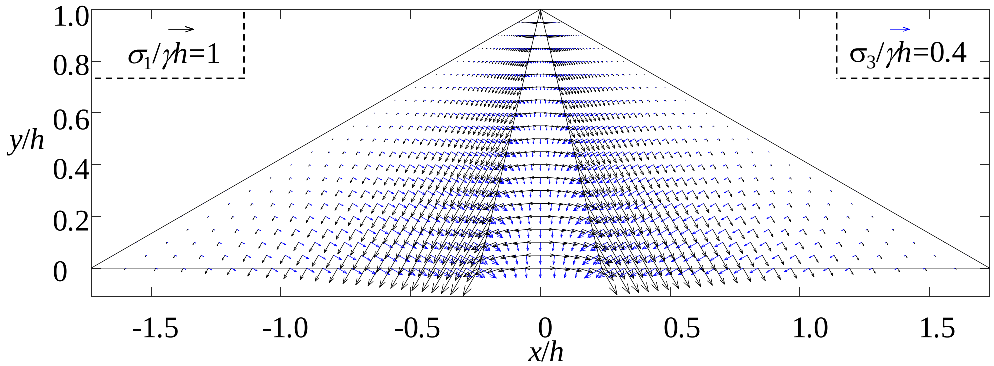

Fig. 18 Trajectories of principal stresses $\sigma_1/\gamma h$ and $\sigma_3/\gamma h$ in planar sand piles with the angle of repose ϕ=30° using incipient failure everywhere solution

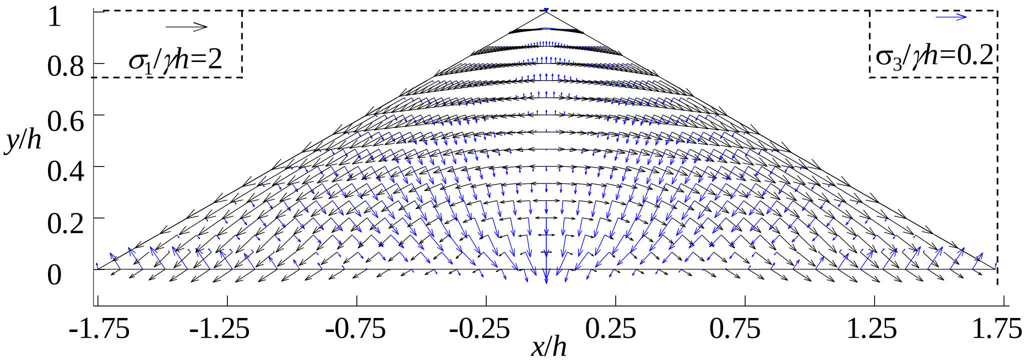

Fig. 19 Trajectories of principal stresses $\sigma_1/\gamma h$ and $\sigma_3/\gamma h$ in planar sand piles with the angle of repose ϕ=30° using the elastic solution

irrespective of a different definition of arching effect from Terzaghi (1943) to Wittmer *et al.* (1997), the kernel features of arching are still preserved.

The trajectories of the principal stresses conjugated to the vertical stress dip in the planar sand pile with the continuum elastic assumption are similar to that of the exact force network calculation proposed by Oron and Herrmann (1998). This point again confirms the feasibility of using the continuum elastic model in studying the arching effect of the granular sand piles.

The arch formation defined in this study obeys the definition proposed by Wittmer *et al.* (1997), nonetheless, the demonstration of the arch formation is different. In Wittmer *et al.* (1997)'s theoretical solution, the direction of the major principal stress is assumed to be constant and fixed. Consequently, the stress dip was found to demonstrate the formulation of the arching effect. By contrast, in the present solution, the stress profiles and the direction of principal stresses are come out simultaneously after numerically solving the governing equations. The arch-like structure in the path of the major principal stress and the stress dip was observed spontaneously to reveal the formation of arch action due to the base deflection. Hence, the physical mechanism responsible for the arching has been sufficiently determined.

4.5 Comparison with incipient failure everywhere (IFE) solution

The load transfer mechanism in the sand piles achieved by the elastic solution is compared with the IFE solution. The IFE solution in the planar and conical sand piles have been elaborately solved by Booker (1969) and Nguyen *et al.* (2019), respectively. The numerical frameworks of the IFE solution proposed by (Nguyen *et al.* 2019) are inherited herein to reproduce the stress profiles at the base of the sand piles. Note that the magnitude of the base deflection in the elastic model is selected to achieve the same value of minimum pressure at the centerline with the IFE solution.

The present stress profiles in the sand piles resting on the rigid base are similar to the IFE solution under alleged active condition (Savage 1998). However, once the base deflects the stress state in the sand piles is analogous to the IFE solution under the passive condition (Booker 1969). A comparison between such two solutions shown in Fig. 17 confirms a good agreement of obtained vertical stress by the continuum elastic model and the IFE solution under the active condition. Whereas, the discrepancy of the vertical stress distribution between the elastic model with base deflection and the IFE solution under passive condition is significant. The elastic solution demonstrates a gradual change of the vertical stress profile while the IFE solution exhibits an abrupt change on the line of stress discontinuity. For obvious difference between two solutions, the trajectories of the principal stresses for the stress profile are plotted in Figs. 18 and 19 and Figs. 20 and 21 for the planar and conical sand piles, respectively.

As seen the connected path of the most compressive principal stress in both solutions is displayed as an arch-like structure. It can be concluded that both solutions have

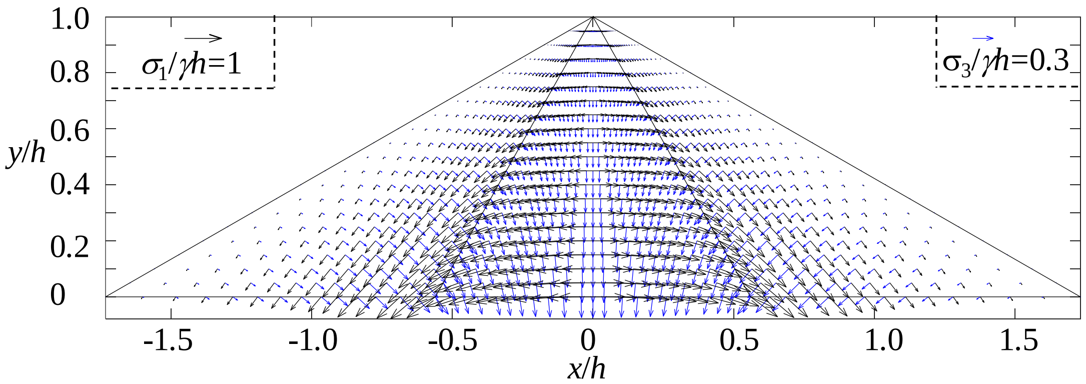

Fig. 20 Trajectories of principal stresses $\sigma_1/\gamma h$ and $\sigma_3/\gamma h$ in conical sand piles with the angle of repose ϕ=30° using incipient failure everywhere solution

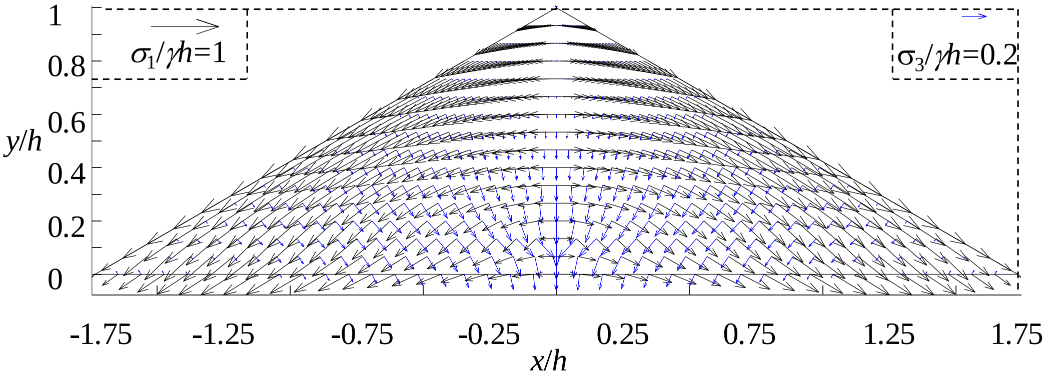

Fig. 21 Trajectories of principal stresses $\sigma_1/\gamma h$ and $\sigma_3/\gamma h$ in conical sand piles with the angle of repose ϕ=30° using the elastic solution

successfully characterized the formation of arch action in the sand piles. However, there are some differences between them in tracking the trajectory of the most compressive principal stress. Firstly, the connected path stemmed from the IFE solution exhibited an abrupt change in direction. The change takes place on the line of stress discontinuity. The hyperbolic governing equations are established based on the assumption that everywhere in sand piles is on the verge of incipient failure obeying the Mohr-Coulomb criterion in association with the self-similarity assumption. Therefore, the basal boundary condition is not important and eliminated in the governing equations. The solution of IFE is achieved by repeatedly estimating the location of the line of stress discontinuity and matching the solution from the traction-free surface to the centerline by integrating the governing equations until achieving the direction of major principal stress is exactly horizontal (Nguyen *et al.* 2019). On the contrary, in the present model, the basal boundary condition is directly taken effect into the elliptic governing equations to solve for stress and strain in the sand piles. Moreover, the direction of the major principal stress on the traction-free slope is also different. In particularly, in the elastic solution, the direction of the major principal stress is exactly coincident with the traction-free slopes; whereas, that of the IFE solution seems to be rotated from the slope surface at an angle of (π/4-ϕ/2). In granular mechanics, the slope surface of a sand heap made of dry cohesionless sand inclined at a repose angle is also a slip-line. Thus, the direction of the major principal stress is rotated from the slope to the angle of (π/4-ϕ/2) as elaborately explained by Nguyen and Pipatpongsa (2020). Physically, granular media of constant bulk unit weight is modelled as a continuous media locked together by friction, with the slip condition occurring in a thin layer above stable slopes. Hence, the shear stress induced by the slip plane could rotate the axis of the major principal stress neighboring to the sliding slope from the direction parallel to the free surface. Being similar to the FPA solution in which, the direction of the major principal stress is presumably decided to establish the hyperbolic governing equation, the IFE solution also take the alleged passive condition whereby the direction of principal stress is determined at the centerline. Hence, such theoretical solutions might be encountered difficulty in seeking mechanistic justification (Savage 1998). Thus, by revealing the stress dip and visualizing the arch-like structure of the connected trajectory of major principal stress in sand pile subjected to base deflection, this study tries to sufficiently determine the physical mechanism responsible for the arching.

4.6 The effect of geometrical non-linearity on the stress dip in sand piles

The vertical stress dip in the planar and conical piles obtained from the linear elasticity and geometrically non-linear elasticity are compared. Interestingly, two models produce an insignificant discrepancy until the maximum base deflection (Δ/h) underneath the apex, illustrated in Fig.

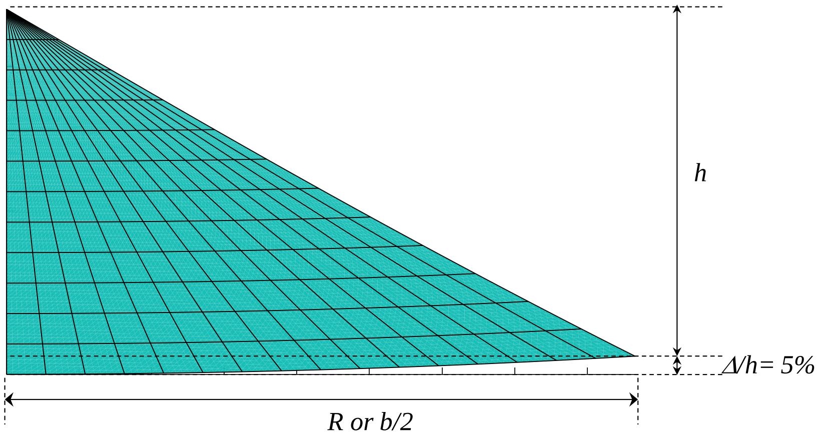

Fig. 22 The shape of the sand piles once the base deflection of 5%

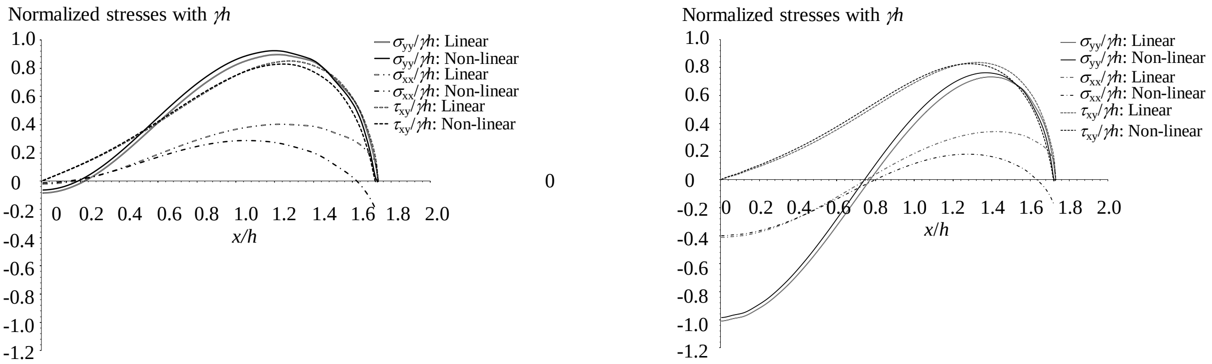

(a) Symmetric planar sand pile (b) Axisymmetric conical sand pile

Fig. 23 Discrepancy in stress redistribution in sand piles between linear and non-linear elasticity with Δ/h=5%

22, is over 5% as shown in Fig. 23.

Once the magnitude of base deflection exceeds that amount, the difference in stress redistribution stemmed from such two models are significant. Without considering the effect of geometrical non-linearity, the base deflection will produce a more pronounced stress dip.

5. Conclusions

The geometrically non-linear isogeometric analysis has been successfully applied in both planar and conical sand piles. Some traits of the load transfer mechanism in the sand piles under the base deflection are summarized as follows:

- The base deflection initiates the stress dip and consequently promotes the shear stress mobilization at the base of the sand piles. The amount of stress dip at the centerline and the shear stress mobilization is directly proportional to the magnitude of the base deflection.
- With the same input data, e.g., height, angle of repose, amount of base deflection, the stress redistribution in the conical sand pile is more sensitive to the base deflection than that of planar one.
- Without stress dip in the case of the rigid base, a weak arch action is proved to appear in the sand piles at the initial condition of the rigid base by showing an arch-like structure in the trajectory of the most compressive principal stress. Thereafter, direction of the most compressive principal stress starts rotating right after imposing the base deflection. Its rotation has intensified the arch action in the sand piles, resulting a pronounced stress dip as well as significant shear stress mobilization at the base. Hence, the concept of arch action, proposed by Wittmer *et al.* (1997), has been elaborately elucidated in this study by visually demonstrating the inclination of force chain in the sand piles corresponding to the magnitude of base deflection. Thus, the physical mechanism responsible for the arching has been elaborately determined and the concept of the arching effect is elaborately elucidated.
- Irrespective of the different definition of the arching effect proposed by Terzaghi (1943) and Wittmer *et al.* (1997), the kernel feature of soil arching in the sand piles is preserved by showing the significant shear stress mobilization accounting for the stress dip in the central vicinity.
- The present results, e.g., the stresses profiles are in good agreement with the available experimental data. Furthermore, the vertical stress profiles at the base of the sand piles are satisfied with the weight balance condition. The validation and verification conclude the reasonability of utilizing IGA in numerical modelling of the sand pile problems.
- The discrepancy in the results of stress redistribution stemmed from the linear and geometrically non-linear

analysis is insignificant until the magnitude of base deflection is over 5%. As observed, the non-linear analysis gains a milder stress dip as compared to the linear one.

References

Abdelrahman, A.A., Esen, I., Özarpa, C. and Eltaher, M.A. (2021), "Dynamics of perforated nanobeams subject to moving mass using the nonlocal strain gradient theory", *Appl. Math. Model.*, **96**, 215-235. https://doi.org/10.1016/j.apm.2021.03.008.

Ai, J., Chen, J.F. and Ooi, J.Y. (2013), "Finite element simulation of the pressure dip in sandpiles", *Int. J. Solid Struct.*, **50**(6), 981-995. https://doi.org/10.1016/j.ijsolstr.2012.12.006.

Ai, J., Chen, J.F., Rotter, J.M. and Ooi, J.Y. (2010), "Numerical and experimental studies of the base pressures beneath stockpiles", *Granul. Matter*, **13**(2), 133-141. https://doi.org/10.1007/s10035-010-0215-6.

Almitani, K.H., Abdelrahman, A.A. and Eltaher, M.A. (2020), "Influence of the perforation configuration on dynamic behaviors of multilayered beam structure", *Structures,* **28**, 1413-1426. https://doi.org/10.1016/j.istruc.2020.09.055.

Alnujaie, A., Akbas, S.D., Eltaher, M.A., Assie, A. (2021), "Forced vibration of a functionally graded porous beam resting on viscoelastic foundation", *Geomech. Eng.*, **24**(1), 91-103. https://doi.org/10.12989/gae.2021.24.1.091.

Angelillo, M., Babilio, E., Fortunato, A., Lippiello, M. and Montanino, A. (2016), "Analytic solutions for the stress field in static sandpiles", *Mech. Mater.*, **95**, 192-203. https://doi.org/10.1016/j.mechmat.2016.01.015.

Atman, A.P., Brunet, P., Geng, J., Reydellet, G., Claudin, P., Behringer, R.P. and Clement, E. (2005), "From the stress response function (back) to the sand pile "dip"", *Eur. Phys. J. E Soft Matter*, **17**(1), 93-100. https://doi.org/10.1140/epje/i2005-10002-2.

Bashiri, A.H., Akbas, S.D., Abdelrahman, A.A., Assie, A., Eltaher, M.A. and Mohamed, E.F (2021), "Vibration of multilayered functionally graded deep beams under thermal load", *Geomech. Eng.*, **24**(6), 545-557. https://doi.org/10.12989/gae.2021.24.6.545.

Bi, G. (2017), "Generalized stress field in granular soils heap with Rayleigh-Ritz method", *J. Rock Mech. Geotech. Eng.*, **9**(1), 135-149. https://doi.org/10.1016/j.jrmge.2016.07.007.

Booker, J.R. (1969), "Applications of the theory of plasticity to cohesive-frictional soils", Ph.D. Dissertation, University of Sydney, Sydney, Australia.

De Luycker, E., Benson, D.J., Belytschko, T., Bazilevs, Y. and Hsu, M.C. (2011), "X-FEM in isogeometric analysis for linear fracture mechanics", *Int. J. Numer. Meth. Eng.*, **87**(6), 541-565. https://doi.org/10.1002/nme.3121.

Eltaher, M.A., Alsulami and R. and Wagih, A. (2021), "On the evolution of energy dissipation in dispersed composite laminates under out-of-plane loading", *Compos. Part B Eng.*, **216**, 108864. https://doi.org/10.1016/j.compositesb.2021.108864.

Esen, I., Abdelrahman, A.A. and Eltaher, M.A. (2020), "Dynamics analysis of timoshenko perforated microbeams under moving loads", *Eng. Comput.*, 1-17. https://doi.org/10.1007/s00366-020-01212-7.

Esen, I., Eltaher, M.A. and Abdelrahman, A.A. (2021), "Vibration response of symmetric and sigmoid functionally graded beam rested on elastic foundation under moving point mass", *Mech. Based Des. Struct. Machines*, 1-25. https://doi.org/10.1080/15397734.2021.1904255.

Girijavallabhan, C.V. and Reese, L.C. (1968), "Finite-element method for problems in soil mechanics", *J. Soil Mech. Found. Div.*, **94**(2), 473-496. https://doi.org/10.1061/JSFEAQ.0001107.

Handy, R.L. (1985), "The arch in soil arching", *J. Geotech. Eng.*, **111**(3), 302-318. https://doi.org/10.1061/(ASCE)0733-9410(1985)111:3(302).

Horabik, J., Parafiniuk, P. and Molenda, M. (2017), "Discrete element modelling study of force distribution in a 3D pile of spherical particles", *Powder Technol.*, **312**, 194-203. https://doi.org/10.1016/j.powtec.2017.02.048.

Hughes, T.J.R., Cottrell, J.A. and Bazilevs, Y. (2005), "Isogeometric analysis: CAD, finite elements, NURBS, exact geometry and mesh refinement", *Comput. Meth. Appl. Mech. Eng.*, **194**(39-41), 4135-4195. https://doi.org/10.1016/j.cma.2004.10.008.

Jaouhar, E.M., Li, L. and Aubertin, M. (2018), "An analytical solution for estimating the stresses in vertical backfilled stopes based on a circular arc distribution", *Geomech. Eng.*, **15**(3), 889-898. https://doi.org/10.12989/gae.2018.15.3.889.

Jeong, H.Y. and Moore, I. (2010), "Calculations for central stress minimum under sand piles using continuum analysis", *ZAMM-J. Appl. Math. Mech.*, **90**(1), 65-71. https://doi.org/10.1002/zamm.200800025.

Lee, I.M., Kim, D.H., Kim, K.Y. and Lee, S.W. (2016), "Earth pressure on a vertical shaft considering the arching effect in c-ϕ soil", *Geomech. Eng.*, **11**(6), 879-896. https://doi.org/10.12989/gae.2016.11.6.879.

Lee, I.K. and Herington, J.R. (1971), "Stresses beneath granular embankments", *Proceedings of the 1st Australia–NewZealand Conference on Geomechanics*, Melbourne, Australia.

Lee, S.W. (2019), "Experimental study on effect of underground excavation distance on the behavior of retaining wall", *Geomech. Eng.*, **17**(5), 413-420. https://doi.org/10.12989/gae.2019.17.5.413.

Li, W., Nguyen-Thanh, N. and Zhou, K. (2018), "Geometrically nonlinear analysis of thin-shell structures based on an isogeometric-meshfree coupling approach", *Comput. Meth. Appl. Mech. Eng. Comput.*, **336**, 111-134. https://doi.org/10.1016/j.cma.2018.02.018.

Liu, Y.Y., Yeung, A.T., Zhang, D.L. and Li, Y.R. (2017), "Experimental study on the effect of particle shape on stress dip in granular piles", *Powder Technol.*, **319**, 415-425. https://doi.org/10.1016/j.powtec.2017.07.021.

Marais, G.V.R. (1969), "Stresses in wedges of cohesionless materials formed by free discharge at the Apex", *J. Eng. Industry*, **91**(2), 345-352.

Matuttis, H.-G. (1998), "Simulation of the pressure distribution under a two-dimensional heap of polygonal particles", *Granul. Matter*, **1**(2), 83-91. https://doi.org/10.1007/s100350050013.

Matuttis, H.G. and Schinner, A. (1999), "Influence of the geometry on the pressure distribution of granular heaps", *Granul. Matter*, **1**(4), 195-201. https://doi.org/10.1007/s100350050025.

McBride, W. (2006), "Base pressure measurements under a scale model stockpile", *Particul. Sci. Technol.*, **24**(1), 59-70. https://doi.org/10.1080/02726350500403264.

Meena, N.K., Nimbalkar, S., Fatahi, B. and Yang, G. (2020), "Effects of soil arching on behavior of pile-supported railway embankment: 2D FEM approach", *Comput. Geotech.*, **123**, 103601. https://doi.org/10.1016/j.compgeo.2020.103601.

Michalowski, R.L. and Park, N. (2004), "Admissible stress fields and arching in piles of sand", *Géotechnique*, **54**(8), 529-538. https://doi.org/10.1680/geot.2004.54.8.529.

Modaressi, A., Boufellouh, S. and Evesque, P. (1999), "Modeling of stress distribution in granular piles: Comparison with centrifuge experiments", *Chaos*, **9**(3), 523-543. https://doi.org/10.1063/1.166427.

Moradi, G. and Abbasnejad, A. (2015), "Experimental and numerical investigation of arching effect in sand using modified

Mohr Coulomb", *Geomech. Eng.*, **8**(6), 829-844. http://doi.org/10.12989/gae.2015.8.6.829.

Nguyen-Thanh, N., Li, W., Huang, J. and Zhou, K. (2020), "Adaptive higher-order phase-field modeling of anisotropic brittle fracture in 3D polycrystalline materials", *Comput. Meth. Appl. Mech. Eng.*, **372**, 113434. https://doi.org/10.1016/j.cma.2020.113434.

Nguyen-Thanh, N., Nguyen-Xuan, H., Bordas, S.P.A. and Rabczuk, T. (2011), "Isogeometric analysis using polynomial splines over hierarchical T-meshes for two-dimensional elastic solids", *Comput. Meth. Appl. Mech. Eng.*, **200**(21-22), 1892-1908. https://doi.org/10.1016/j.cma.2011.01.018.

Nguyen-Thanh, N., Li, W., Huang, J., Srikanth, N. and Zhou, K. (2019), "An adaptive isogeometric analysis meshfree collocation method for elasticity and frictional contact problems", *Int. J. Numer. Meth. Eng.*, **120**(2), 209-230. https://doi.org/10.1002/nme.6132.

Nguyen, T. and Pipatpongsa, T. (2020), "Plastic behaviors of asymmetric prismatic sand heaps on the verge of failure", *Mech. Mater.*, **151**, 103624. https://doi.org/10.1016/j.mechmat.2020.103624.

Nguyen, T., Pipatpongsa, T., Kitaoka, T. and Ohtsu, H. (2018), "Numerical investigation of stress dip in embankments using elastic model based on isogeometric analysis method", *J. Jap. Soc. Civ. Eng.*, **74**(2), 349-360. https://doi.org/10.2208/jscejam.74.I_349.

Nguyen, T., Pipatpongsa, T., Kitaoka, T. and Ohtsu, H. (2019), "Stress distribution in conical sand heaps at incipient failure under active and passive conditions", *Int. J. Solids Struct.*, **168**, 1-12. https://doi.org/10.1016/j.ijsolstr.2018.04.001.

Nguyen, V.P., Anitescu, C., Bordas, S.P.A. and Rabczuk, T. (2015), "Isogeometric analysis: An overview and computer implementation aspects", *Math. Comput. Simul.*, **117**, 89-116. https://doi.org/10.1016/j.matcom.2015.05.008.

Nguyen, V.P., Rabczuk, T., Bordas, S. and Duflot, M. (2008), "Meshless methods: A review and computer implementation aspects", *Math. Comput. Simul.*, **79**(3), 763-813. https://doi.org/10.1016/j.matcom.2008.01.003.

Okamura, M., Tamamura, S. and Yamamoto, R. (2013), "Seismic stability of embankments subjected to pre-deformation due to foundation consolidation", *Soils Found.*, **53**(1), 11-22. https://doi.org/10.1016/j.sandf.2012.07.015.

Ooi, J., Ai, J., Zhong, Z., Chen, J. and Rotter, J. (2008), *Progressive Pressure Measurements beneath a Granular Pile with and without Base Deflection*, in *Structures and Granular Solids*, CRC Press, 87-92.

Oron, G. and Herrmann, H.J. (1998), "Exact calculation of force networks in granular piles", *Phys. Rev. E*, **58**(2), 2079-2089. https://doi.org/10.1103/PhysRevE.58.2079.

Parry, R.H. (1954), "Measurement of pressure distribution across the base of triangular section granular masses", Ph.D. Dissertation, University of Melbourne, Melbourne, Australia.

Peters, J.F., Muthuswamy, M., Wibowo, J. and Tordesillas, A. (2005), "Characterization of force chains in granular material", *Phys. Rev. E*, **72**(4), 041307.

Piegl, L. and Tiller, W. (1995), *The NURBS Book*, Springer-Verlag Berlin Heidelberg, Germany.

Pipatpongsa, T., Matsushita, T., Tanaka, M., Kanazawa, S. and Kawai, K. (2014), "Theoretical and experimental studies of stress distribution in wedge-shaped granular heaps", *Acta Mech. Solid. Sin.*, **27**(1), 28-40. https://doi.org/10.1016/S0894-9166(14)60014-8.

Pipatpongsa, T., Nakamura, J., Borely, C. and Khosravi, M. (2014), "Numerical lower bound limit analyses of sand heap subjected to basal settlement with hysteretic reversals", *Proceedings of the 14th International Conference of International Association for Computer Methods and Recent Advances in Geomechanics*, Kyoto, Japan, September.

Savage, S.B. (1998), *Modeling and Granular Material Boundary Value Problems*, in *Physics of Dry Granular Media*, Springer, Dordrecht, Germany. 25-96.

Smid, J. and Novosad, J. (1981), "Pressure distribution under heaped bulk solids", *Proceedings of the 1981 Powtech Conference*, Birmingham, U.K., March.

Terzaghi, K. (1943), *Theoretical Soil Mechanics*, Wiley and Sons, Inc., New York, U.S.A.

Tran, L.V., Lee, J., Nguyen-Van, H., Nguyen-Xuan, H. and Wahab, M.A. (2015), "Geometrically nonlinear isogeometric analysis of laminated composite plates based on higher-order shear deformation theory", *Int. J. Non-Lin. Mech.*, **72**, 42-52. https://doi.org/10.1016/j.ijnonlinmec.2015.02.007.

Tran, L.V. and Niiranen, J. (2020), "A geometrically nonlinear Euler–Bernoulli beam model within strain gradient elasticity with isogeometric analysis and lattice structure applications", *Math. Mech. Complex Syst.*, **8**(4), 345-371. https://doi.org/10.2140/memocs.2020.8.345

Tran, L.V., Phung-Van, P., Lee, J., Wahab, M.A. and Nguyen-Xuan (2016), "Isogeometric analysis for nonlinear thermomechanical stability of functionally graded plates", *Compos. Struct.*, **140**, 655-667. https://doi.org/10.1016/j.compstruct.2016.01.001.

Trollope, D.H. (1956), "The stability of wedges of granular materials", University of Melbourne, Melbourne, Austalia.

Trollope, D.H. and Burman, B.C. (1980), "Physical and numerical experiments with granular wedges", *Géotechnique*, **30**(2), 137-157. https://doi.org/10.1680/geot.1980.30.2.137.

Wensrich, C. and Katterfeld, A. (2012), "Rolling friction as a technique for modelling particle shape in DEM", *Powder Technol.*, **217**, 409-417. https://doi.org/10.1016/j.powtec.2011.10.057.

Wittmer, J.P., Cates, M.E. and Claudin, P. (1997), "Stress propagation and arching in static sandpiles", *J. Physique I*, **7**(1), 39-80. https://doi.org/10.1051/jp1:1997126.

Wittmer, J.P., Claudin, P., Cates, M.E. and Bouchaud, J.P. (1996), "An explanation for the central stress minimum in sand piles", *Nature*, **382**(6589), 336-338. https://doi.org/10.1038/382336a0.

Yang Y., Tang X., Zeng H., Liu Q. and He L. (2016), "Three-dimensional fracture propagation with numerical manifold method", *Eng. Anal. Bound. Elem.*, **72**, 65-77. https://doi.org/10.1016/j.enganabound.2016.08.008.

Yang Y., Tang X., Zeng H., Liu Q. and and Liu Z. (2018), "Hydraulic fracturing modeling using the enriched numerical manifold method", *Appl. Math. Model.*, **53,** 462-486. https://doi.org/10.1016/j.apm.2017.09.024.

Yang Y., Sun G., Zeng H. and Qi Y. (2019), "Investigation of the sequential excavation of a soil-rock-mixture slope using the numerical manifold method", *Eng. Geol.*, **256**, 93-109. https://doi.org/10.1016/j.enggeo.2019.05.005.

Yang Y., Wu W. and Zeng H. (2021), "Stability analysis of slopes using the vector sum numerical manifold method", *B. Eng. Geol. Environ.*, **80**, 345-352. https://doi.org/10.1007/s10064-020-01903-x.

Zhou, Z., Zou, R., Pinson, D. and Yu, A. (2014), "Angle of repose and stress distribution of sandpiles formed with ellipsoidal particles", *Granul. Matter*, **16**(5), 695-709. https://doi.org/10.1007/s10035-014-0522-4.

Wu W., Yang Y. and Zeng H. (2020), "Enriched mixed numerical manifold formulation with continuous nodal gradients for dynamics of fractured poroelasticity", *Appl. Math. Model.*, **86**, 225-258. https://doi.org/10.1016/j.apm.2020.03.044.

GC

Appendix

From the rectangular stress components in the sand piles, the principal stresses are given by

$$\sigma_1 = \frac{\sigma_{xx}+\sigma_{yy}}{2} + \sqrt{\left(\frac{\sigma_{xx}-\sigma_{yy}}{2}\right)^2 + \left(\tau_{xy}\right)^2}$$
$$\sigma_3 = \frac{\sigma_{xx}+\sigma_{yy}}{2} - \sqrt{\left(\frac{\sigma_{xx}-\sigma_{yy}}{2}\right)^2 + \left(\tau_{xy}\right)^2} \qquad \text{(A1)}$$

Herein, σ_1 is the major principal stress while σ_3 is the minor one. Since the stresses are commonly compressive in the sand pile problems, the major principal stress is always the most compressive principal stress.

In particular, for the planar sand pile, the constitutive equation can be simplified as

$$\begin{Bmatrix} \sigma_{xx} \\ \sigma_{yy} \\ \tau_{xy} \end{Bmatrix} = \frac{E}{(1+\mu)(1-2\mu)} \begin{bmatrix} 1-\mu & \mu & 0 \\ \mu & 1-\mu & 0 \\ 0 & 0 & 0.5-\mu \end{bmatrix} \begin{Bmatrix} \varepsilon_{xx} \\ \varepsilon_{yy} \\ \gamma_{xy} \end{Bmatrix} \qquad \text{(A2)}$$

in which E is Young's modulus, μ is Poisson's ratio. Meanwhile for the axisymmetric conical sand pile, it can be transformed as

$$\begin{Bmatrix} \sigma_{xx} \\ \sigma_{yy} \\ \tau_{xy} \\ \sigma_{\theta\theta} \end{Bmatrix} = \frac{E}{(1+\mu)(1-2\mu)} \begin{bmatrix} 1-\mu & \mu & 0 & \mu \\ \mu & 1-\mu & 0 & \mu \\ 0 & 0 & 0.5-\mu & 0 \\ \mu & \mu & 0 & 1-\mu \end{bmatrix} \begin{Bmatrix} \varepsilon_{xx} \\ \varepsilon_{yy} \\ \gamma_{xy} \\ \varepsilon_{\theta\theta} \end{Bmatrix} \qquad \text{(A3)}$$

The strain matrices are given by

$$\mathbf{B}_A^L = \begin{bmatrix} N_{A,x} & 0 \\ 0 & N_{A,y} \\ N_{A,y} & N_{A,x} \\ N_A/x & 0 \end{bmatrix}, \ \mathbf{B}_{\alpha_A}^{NL} = \begin{bmatrix} \mathbf{A}_{\alpha_A} \\ \mathbf{0} \end{bmatrix} \mathbf{B}_{\alpha_A}, \ \mathbf{B}_\theta^{NL} = \frac{u}{x^2} \begin{bmatrix} \mathbf{0} \\ \mathbf{B}_{\theta_A} \end{bmatrix} \qquad \text{(A4)}$$

in which

$$\mathbf{B}_{\alpha_A} = \begin{bmatrix} \delta_{\alpha u} N_{A,x} & \delta_{\alpha v} N_{A,x} \\ \delta_{\alpha u} N_{A,y} & \delta_{\alpha v} N_{A,x} \end{bmatrix} \quad \text{and} \qquad \text{(A5)}$$
$$\mathbf{B}_{\theta_A} = \begin{bmatrix} N_A & 0 \end{bmatrix}$$

The tangent stiffness matrix, $\mathbf{K}_T$, is obtained from derivative of the residual force with respect to nodal vector as follows

$$\mathbf{K}_T = \frac{\partial \boldsymbol{\varphi}}{\partial \mathbf{d}} = 2\pi \int_\Omega \left(\mathbf{B}^T \frac{\partial \hat{\boldsymbol{\sigma}}}{\partial \mathbf{d}} + \frac{\partial \mathbf{B}^T}{\partial \mathbf{d}} \hat{\boldsymbol{\sigma}} \right) x d\Omega = \mathbf{K}^{NL} + \mathbf{K}^g \qquad \text{(A6)}$$

where $\mathbf{K}^{NL}$, $\mathbf{K}^g$ are the nonlinear and geometric stiffness matrices, respectively

$$\mathbf{K}^{NL} = 2\pi \int_\Omega \left(\mathbf{B}^L + \mathbf{B}_\alpha^{NL} + \mathbf{B}_\theta^{NL} \right)^T \mathbf{C} \left(\mathbf{B}^L + \mathbf{B}_\alpha^{NL} + \mathbf{B}_\theta^{NL} \right) x \mathrm{d}\Omega \qquad \text{(A7)}$$

$$\mathbf{K}^g = 2\pi \int_\Omega \left(\left(\mathbf{B}_\alpha^g\right)^T \mathbf{N}_0 \mathbf{B}_\alpha^g + \left(\mathbf{B}_\theta\right)^T \frac{\sigma_{\theta\theta}}{x^2} \mathbf{B}_\theta \right) x \mathrm{d}\Omega \qquad \text{(A8)}$$

in which the stresses matrix $\mathbf{N}_0$ is arranged from in-plane stress obtained from Eq. (11) as follows

$$\mathbf{N}_0 = \begin{bmatrix} \sigma_{xx} & \tau_{xy} \\ \tau_{xy} & \sigma_{yy} \end{bmatrix} \qquad \text{(A9)}$$